Volum 36, N s. 1–3
May 1991
ISS
Editor: Ein

ENG

E

ultramicroscopy

An International Journal affiliated with EMSA, ISEM, SCANDEM, NVEM, SGOEM, SIME-SM, DGE, MSC and ASEM

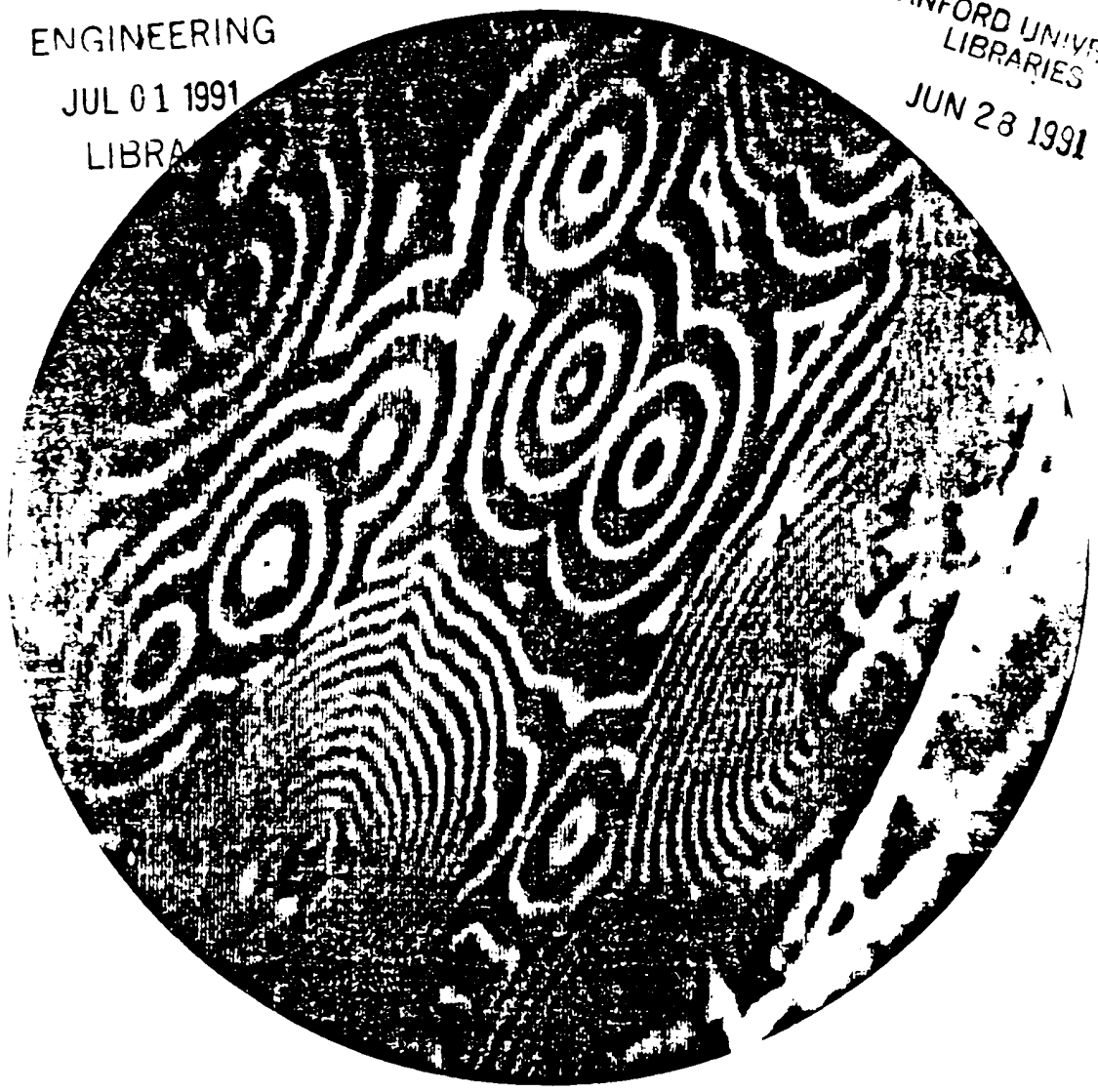

This issue is part of the 1990 subscription program
To be followed by Volume 35, Number 3

NORTH-HOLLAND

ULTRDG 36(1-3) 1-274 (1991)

Ultramicroscopy 36 (1991) 63–75
North-Holland

Scanning versus direct imaging emission microscopy .*

Lee H. Veneklasen [1]
Physikalisches Institut der TU Clausthal, W-3392 Clausthal-Zellerfeld, Germany

Received 17 August 1990; at Editorial Office 7 January 1991

The theoretical performance of an optimized direct imaging emission microscope is compared with a scanning Auger microprobe for the chemical mapping of surfaces at high resolution. The comparison criterion is visibility or image signal-to-noise ratio versus actual resolution. A model is developed to include specimen parameters, illumination conditions, and collection efficiency factors. Optimum conditions for gun brightness, Coulomb interactions and dose-limited cases are derived. The model is evaluated to obtain an estimate of future possibilities. The scanning system offers higher collection efficiency, but its advantage is more than offset by the advantages of parallel illumination and detection of direct images containing many pixels. The imaging system seems to offer better resolution and faster data collection in most cases.

1. Introduction

There are two different electron microscopes that can use Auger electrons for the chemical mapping of surfaces. The scanning Auger microprobe (SAM) is well known. The low-energy electron microscope (LEEM) is known for its studies of surface structure using elastic backscatter imaging and LEED diffraction [1,2], but it has not yet been applied to the spectroscopic mapping of surfaces [3]. This instrument is the surface-imaging equivalent of a transmission electron microscope. With the addition of an imaging energy analyzer, an inelastic image from characteristic Auger peaks may be selected, and the energy-loss spectroscopy techniques used in TEM may be applied to surfaces.

The primary challenge in spectroscopic imaging is to acquire adequate image statistics during an acceptable exposure time. Chemical information comes from weak peaks within a diffuse background of secondary and backscatter electrons. While the contrast may be enhanced by synchronous detection of difference signals, the background contributes the majority of image noise. The criteria for the "visibility" of a chemical "feature" is that its resolution element (pixel) may be distinguished from an adjacent pixel of different composition. Thus the signal-to-noise ratio of a pixel, as a function of resolution, image integration time, and total image pixel count, is the measure of visibility of a spectroscopic image.

Both the spatial and the temporal distributions of surface material are of interest, and wide bandwidth for the determination of both is desired. Problems arise when both are needed simultaneously, for example when observing epitaxial growth or surface diffusion. Spectroscopy of large fields allows average composition to be determined quickly. However, many phenomena also depend upon how material is distributed, e.g., in clusters, monolayers, or concentrations along topographic or crystalline boundaries. Since image statistics must be gathered from smaller areas, temporal resolution is sacrificed. Thus high spatial resolution in a short time interval is the primary goal.

In a scanning instrument, the current in the probe decreases rapidly with the probe size (reso-

* This work was supported by a grant from the Volkswagen Foundation.

[1] Present address: KLA Instruments Inc., 3520 Bassett Street, Santa Clara, CA 95052, USA.

0304-3991/91/$03.50

lution), generating less signal in a given time interval. In a direct-imaging instrument, the problem is reversed. While many pixels may be illuminated in parallel, allowing high currents to be used, it becomes increasingly difficult to efficiently detect the signal from each pixel. In an imaging system, resolution requirements limit the aperture angle of the detection optics. As the resolution improves, a larger fraction of the signal is lost. Since image statistics ultimately depend upon the number of characteristic electrons *recorded* in the available time interval, it is not immediately obvious which kind of imaging is more favorable.

These tradeoffs will be explored in detail. First, a model for both instruments is proposed. The model makes a minimum distinction between scanning and imaging configurations, leaving a maximum number of free parameters. Optimization techniques for the two instruments are developed from the model, and the basic differences are pointed out. The final instrument-specific equations for signal-to-noise ratio versus resolution are evaluated, using numbers reflecting the author's (it is hoped) realistic estimation of future design goals. The model may be equally well applied to existing systems.

2. The SAM system

An advanced scanning Auger microprobe for high-speed, high-resolution mapping, shown in fig. 1, would probably use a cylindrical mirror analyzer (CMA), and a coaxial field emission gun with a small conical magnetic objective lens. In order to allow Auger electrons to pass into the CMA annulus, it is usually necessary that the region in front of the lens be free of large electric and magnetic fields. This forbids the use of immersion lenses which might otherwise be desirable, but also allows a wide range of surfaces to be observed. Viewed as a system, the most important instrumental parameters are the current versus spot size of the scanning probe and the collection efficiency of the CMA at the necessary energy resolution.

To detect a weak signal in the strong background, the analyzer energy window is usually alternated between the peak and adjacent background spectrum. The transmitted beam is normalized to a beam current reference signal from an annular aperture to eliminate field emission noise, and then synchronously detected. Spatial information is gathered serially, one pixel after the other. One example of such an instrument is described in ref. [5].

3. The spectroscopic LEEM

In this work, the term LEEM refers to all instruments that use a bidirectional beam cathode lens to form *direct* images of low-energy reflected or re-emitted electrons. The spectroscopic or analytic LEEM shown in fig. 1 uses a cathode immersion lens to form a direct, unscanned image using characteristic peaks within the secondary emission spectrum. When using Auger peaks excited by electron illumination, the same cathode lens is used to focus illumination on the area of the sample being imaged. Thus a two-way beam path is used in the objective. A magnetic prism separator directs the illumination and imaging beams along separate paths from the gun and into the magnifying image optics. After magnification and energy analysis, the image appears upon an image intensifier. Similar to the SAM, the analyzer window is alternated between peak and background, so that the final display is the difference between signal and background frames. Frames are recorded in real time by a TV camera, averaged and subtracted in an image processor, and displayed on a TV monitor. Full field spectra may also be recorded by scanning the spectrum while summing all pixels in the image frame. Ref. [6] describes a design now under construction.

In the LEEM, the specimen is immersed in a strong electric field. Low-energy electrons leaving the surface are rapidly accelerated to about 20 keV, forming a virtual image behind the sample [7]. The main focusing action occurs during acceleration, very near the sample. The refocusing portion of the objective lens acts upon the accelerated beam, forming a real image at the achromatic plane of the separator. Such an immersion lens has remarkably low aberration because the accel-

Fig. 1. C
magnetic
current
imaging

erating
may b
angles.
be mu
the im
be fav
sampl
the le
high-r
The
illumir
LEEM
diffrac
the sa
lumina
exactly
optics
in this
tron g
sible.
Illu
separa
accord
ments.
plane
plane.

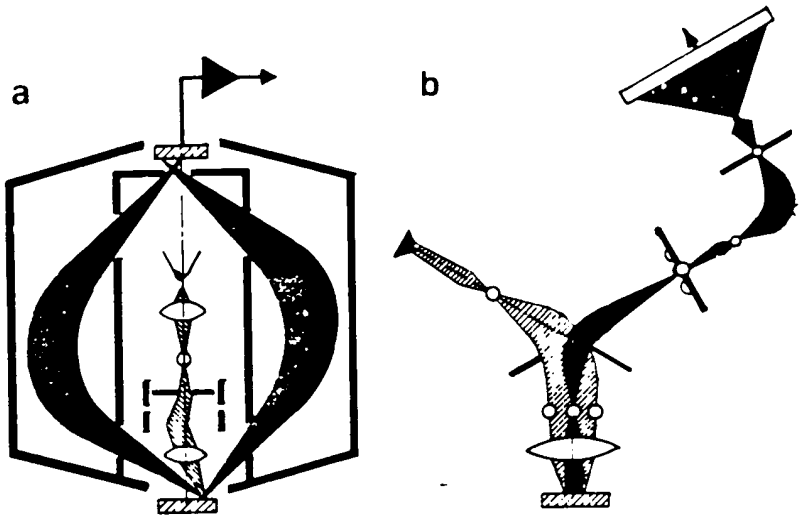

Fig. 1. Concepts of (a) SAM and (b) SPEC LEEM instruments. (a) Scanning Auger microprobe: high brightness F.E. gun, conical magnetic objective lens, CMA analyzer, complementary SEM, low current – high collection, exposure rises with number of pixels, current falls with pixel size. (b) Direct imaging SPEC LEEM: high current LaB_6 gun, electromagnetic immersion objective lens, imaging analyzer, complementary SEM, LEEM, LEED and PEEM, high current – lower collection, exposure independent of number of pixels, current falls slower with pixel size.

erating lens is physically small. High resolution may be obtained using very large initial takeoff angles. This allows the solid angle of collection to be much larger than one might expect. Without the immersion lens, the SPEC LEEM would not be favorable. The primary disadvantage is that the sample surface forms the most important part of the lens, so it must be macroscopically flat for high-resolution imaging.

The immersion lens is also used to achieve high illumination intensity. In contrast to the familiar LEEM, which requires parallel illumination for diffraction contrast, the SPEC LEEM illuminates the sample like a probe-forming system. The illumination disk is a large aberration figure that exactly fills the field of view. The illumination optics are tuned to maximize the current density in this large spot. Using a thermionic LaB_6 electron gun, very high illumination currents are possible.

Illumination and imaging beams are apertured separately. Both these apertures are chosen according to resolution and field-of-view requirements. The image-contrast aperture is placed at a plane conjugate to the objective lens back focal plane, so that it serves as a virtual aperture limiting the acceptance angle at the specimen. The sample is biased at Auger line energy so that the illumination and imaging optics always operate at the same energies (~ 23 and 20 keV, respectively).

In the SPEC LEEM, statistics in each pixel are, in principle, independent of pixel count, because each pixel is exposed for the full image integration time. This is the basic advantage of a full field image system, and it is why light microscopes and TEMs are more popular than their scanning counterparts. However, specimen heating, Coulomb interactions, and collection efficiency effects can significantly reduce this advantage. A detailed analysis is needed to determine the tradeoffs. At the risk of a complex development, the next section will analyze these tradeoffs.

4. Detection statistics in an image pixel

Let N_s be the number of true Auger electrons that reach one pixel of the final image during the time τ that this pixel is exposed. Let N_b be the number of unwanted background electrons in the same or in an adjacent energy window. If the image is the difference between signal and ad-

jacent background exposures, then the total noise is the quadrature sum of the quantum noise $\sqrt{N}$ in both signals. Let the contrast be $N_s/N_b = K$, where for weak Auger lines on a strong background the contrast is much less than one. Using the definition of detection quantum efficiency DQE = $Q \leq 1$ as the ratio of the square of actual, to quantum-noise-limited signal-to-noise ratio, we have the following expression for the square of signal to noise in each pixel:

$$\text{Signal} = (N_s + N_b) - (N_b) = N_s,$$

$$\text{Noise} = \left(\sqrt{N_s + N_b}^2 + \sqrt{N_b}^2\right)^{1/2} \approx \sqrt{2N_b} \quad \text{if} \quad K \ll 1, \tag{1}$$

$$(S/N)^2 = KN_sQ/2.$$

Fig. 2 shows an Auger spectrum from the surface. Quantum yields Y_s for the Auger line alone, and Y_b for the background are in units of percent per primary electron where the line energy is V, and the incident primary energy is V_1 (eV). The yields refer to the emission into the full emission solid angle Ω_s, and natural linewidth ΔE. The contrast is $K = Y_s/Y_b$.

The number N_s of electrons reaching the detector depends upon the product of incident dose (electrons/pixel), the net yield (%), and the collection efficiency $\Omega\,\Delta V/\Omega_s\,\Delta E$ (%). Only half of the total exposure time τ is available for collecting the N_s signal electrons, which will be accounted for in the yield factor below. The specimen yield factor $KY_s/4\Omega_s\,\Delta E$ (percent/sr · eV) combines the specimen-dependent parameters that contribute to the signal-to-noise expression in eq. (1).

The incident flux is the product of flux density, pixel area, and exposure time per pixel. If δ is the size of a resolved pixel, J the current density, τ exposure time, and e the electron charge, then the illumination dose factor is $J\tau\delta^2/e$ (electrons/pixel).

The collection factor $Q\Omega\,\Delta V$ (percent · sr · eV) is the product of the solid angle Ω viewed by the detection and imaging optics, and the energy window ΔV used in the analyzer. We do not assume a priori that this window should be equal to the linewidth. The DQE = Q may be thought of as an attenuation necessary for the detector to be quantum-noise limited. Summarizing the above discussion:

$$\left(\frac{S}{N}\right)^2 = \underbrace{\frac{KY_s}{4\Omega_s\,\Delta E}}_{\substack{\text{yield factor}\\(\text{percent/sr} \cdot \text{eV})}} \times \underbrace{\frac{J\tau\delta^2}{e}}_{\substack{\text{dose factor}\\(\text{electrons/pixel})}} \times \underbrace{Q\Omega\,\Delta V}_{\substack{\text{collection factor}\\(\text{percent} \cdot \text{sr} \cdot \text{eV})}} \left(\frac{\text{electrons}}{\text{pixel}}\right). \tag{2}$$

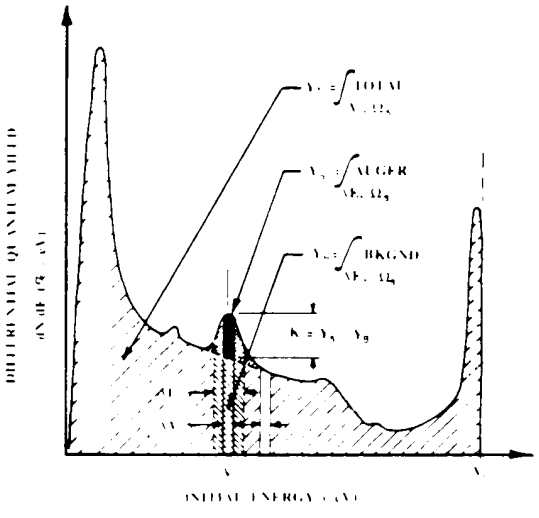

Fig. 2. Definition of parameters from an emission spectrum.

5. Optimizing the instrumental conditions

5.1. Optimizing the yield factor

For a given imaging task, the yield factor is optimized by the choice of spectral line V (eV) and incident illumination energy V_1 (eV), which should be chosen to maximize the entire factor. Contrast is as important as line yield, and in some cases a weaker line with relatively less background may be favored. Similar considerations apply to the choice of incident energy. It also seems desirable to minimize the total yield Y_T of all scattering by appropriate choice of V_1. The presence of substrate peaks adjacent to the line also needs to be

considered, as does the possibility of deviations from a cosine-distributed angular emission.

5.2. Optimizing the dose factor

The essential difference between scanning and direct imaging appears in the dose factor. If a total time T (s) is available for exposure, and a field of $n \times n = n^2$ pixels is to be resolved, then the exposure time τ available for each pixel is

$$\begin{aligned} &\text{for scanning} \quad \tau = T/n^2, \\ &\text{for imaging} \quad \tau = T. \end{aligned} \tag{3}$$

With comparable gun brightness and coherence/current density conditions, the dose factor for direct imaging is n^2 larger. However, in comparing the two instruments, there are several factors that modify this simple view. In particular, inelastic imaging places no inherent constraints upon the parallelism (coherence) of the illumination because secondaries and Augers emerge with an angular distribution that is not correlated with the narrow cone of illumination. The precise goal of the illumination optics is thus to deposit a maximum *current* upon the area being imaged.

In both systems, the illumination is an aberrated image of a source in the electron gun. This source may be characterized by a diameter d_g, and an average brightness $B_i(V_i)$ (A/cm^2 · sr) measured at sample illumination voltage V_i instead of at gun voltage. As shown in fig. 3, the illumination optics images this source on the specimen with a magnification M_i, forming an illumination disk of diameter d_i and angular divergence α_i at the sample. If this disk contains a current I, then by the definition of brightness, $B_i = 4I/\pi^2 d_i^2 \alpha_i^2$. The diameter of the disk is given by the expression:

$$d_i^2 = C_{si}^2 \alpha_i^6 + C_{ci}^2 \alpha_i^2 \, \Delta V_i^2 / V_i^2 + 0.36 K_\lambda^2 / V_i \alpha_i^2 + M_i^2 d_g^2, \tag{4}$$

where C_{si}, C_{ci} are spherical and chromatic aberration coefficients, $K_\lambda = \lambda\sqrt{V} = h/\sqrt{2me} = 12 \times 10^{-8}$ cm $\sqrt{\text{eV}}$ is a voltage-independent wavelength factor. All parameters above are referred to illumination voltage V_i even if the beam has been decelerated from a higher energy. To optimize the current in this spot, we approximately follow the development of Mulvey [8]. For larger spots, spherical and source size terms dominate. The equation is expressed in terms of the acceptance angle α_g of the optics as seen from the gun. α_g is proportional to $M_i \alpha_i$. α_g is then maximized to accept maximum current from the gun. Then optimum magnification, aperture angle and beam current may be expressed in terms of the desired illumination diameter:

$$\begin{aligned} &M_{i,\text{opt}} = 0.87 d_i / d_g, \\ &\alpha_{i,\text{opt}}^2 = 0.63 (d_i / C_{si})^{2/3}, \\ &I = \pi^2 B_i d_i^2 \alpha_{i,\text{opt}}^2 / 4 = 1.55 B_i d_i^{8/2} / C_{si}^{2/3}. \end{aligned} \tag{5}$$

For the scanning system, the dose factor is found by setting the illumination disk equal to the pixel size $d_i \to \delta$, so that the average current density is $J = I/\delta^2$. For imaging we assume that the diameter of the illumination disk is chosen to span the diagonal of a $n \times n$ field so that $J = 4I/\pi d_i^2$ with $d_i = \sqrt{2}\, n\delta$.

The corresponding dose factors are for scanning

$$J\tau\delta^2/e \le 1.55 B_i T \delta^{8/3} / e n^2 C_{si}^{2/3}, \tag{6a}$$

and for imaging

$$J\tau\delta^2/e \le 2.48 B_i T n^{2/3} \delta^{8/3} / e C_{si}^{2/3}. \tag{6b}$$

Although this formulation is correct only for thermionic gun systems, it may be used to fit field

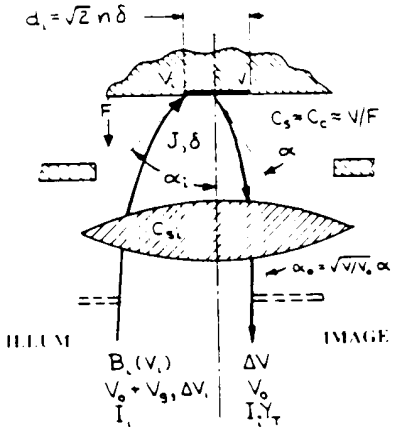

Fig. 3. Objective lens parameters.

emission gun data by using an appropriate "reduced brightness" that accounts for gun lens aberrations and Coulomb interactions. This empirical value may be calculated from the $I(\delta)$ curves of known FE systems [5,9] and applied here. At high currents, the reduced brightness falls drastically, so that FE illumination is not advantageous in a SPEC LEEM.

It seems likely that stochastic Coulomb interactions instead of gun brightness will indirectly limit the useable current in a SPEC LEEM. Their effect is to degrade resolution approximately linearly with the total current in the imaging beam [10]. The imaging current depends upon the product of illumination current and total reflected yield Y_T from the entire illuminated specimen area. This is why it seems desirable to only illuminate the area being imaged. It is probably acceptable to ignore the coaxial illuminating beam itself, because interaction times are short for electrons travelling in the opposite direction. However, image Auger electrons move in a cloud of secondaries and backscatter with similar velocities. Interaction times are longer, and the statistical sample of collisions is smaller, giving rise to stochastic interactions.

To estimate this effect, let the image current $I_i = IY_T$, and assume that resolution δ increases linearly with image current with an *empirical* proportionality factor k (cm/A). Then the total current in the illumination disk is limited to $I \le \delta/k$ for scanning, and to $I \le \delta/kY_T$ for imaging. Calculating the current densities using the disk diameters δ and $\sqrt{2}n\delta$, the interactions-limited dose factors are:

$$\begin{aligned} &\text{for scanning} \quad J\tau\delta^2/e \le 1.0T\delta/ekn^2, \\ &\text{for imaging} \quad J\tau\delta^2/e \le 0.63T\delta/ekY_T n^2. \end{aligned} \tag{7}$$

When formulated in this way, the empirical factor k for the *nonaccelerating* portion of the beam path may be extracted from the electron beam lithography literature, where the edge slope δ in a shaped beam of size d_i has been measured as a function of beam current, path lengths and aperture angles. Fortunately, the accelerating region is very short, and will tentatively be neglected. A complete formulation for two-way, accelerating, polychromatic beams is unavailable, but should be undertaken to determine the limits of the cathode lens LEEM system.

Specimen damage can also limit the useable dose. Let the damage-limited dose $D_{max} = J\tau$ (A · s/cm^2), so the dose factor for both instruments becomes:

$$\text{for scanning and imaging} \quad J\tau\delta^2/e \le D_{max}\delta^2/e. \tag{8}$$

Note that this limit is independent of integration time, and the product JT for imaging and JT/n^2 for scanning is constant. With its higher current, the imaging instrument is faster, but the relative signal-to-noise ratios depend only upon the collection factor when the illumination is limited by damage effects.

5.3. *Optimizing for best resolution*

There are two different ways to set imaging conditions in a spectroscopic instrument. When sample topography and structure as well as composition are of interest, then high-yield secondary and backscatter electrons may be used for high-resolution images. The illumination optics, energy window and aperture angles may be chosen to optimize resolution at the expense of dose and collection efficiency. For chemical mapping, weak Auger lines must be used, and the visibility of small features will usually be limited by the signal-to-noise ratio. Frequently the ultimate resolution cannot be exploited. Facing this situation, it is better to optimize illumination, aperture angles and energy window for a realistic resolution goal. This section will derive expressions for *ultimate* optics-limited resolution without regard for signal statistics. The next section will derive conditions that optimize *collection efficiency* as a function of resolution.

At the low energies V_i, V_i used in Auger systems, ultimate resolution is almost always determined by the balance of chromatic and diffraction terms in eq. (4). In a scanning system, parameters are defined for the illuminating spot V_i, electron gun energy spread ΔV_i, aperture angle α_i, and $d_i = \delta$. By requiring that $\partial\delta/\partial\alpha_i = 0$, opti-

mum aperture angle and minimum resolution are determined. The spot current approaches zero as the demagnification is increased to reduce the effect of finite source size. The collection factor $\Omega\,\Delta V$ in the CMA is not influenced by the choice of illumination conditions. The energy window is usually chosen to include the entire line $\Delta V = \Delta E$, and the analyzer has a fixed acceptance solid angle Ω_A (sr). For high-resolution conditions *for scanning*

$$\begin{aligned} \alpha_{i,\mathrm{opt}}^2 &= 0.6K_\lambda V_i^{1/2}/C_{ci}\,\Delta V_i, \\ \delta_{\min}^2 &= 1.2K_\lambda C_{ci}\,\Delta V_i/V_i^{3/2}, \\ \Omega\,\Delta V &= \Omega_A\,\Delta E. \end{aligned} \tag{9}$$

The same basic lens optimization may be applied to the cathode lens of the imaging system shown in fig. 3, but the beam energy is the Auger line energy V, and the energy spread is not determined by the source, but rather by the *minimum* window of the analyzer $\Delta V_{\min}$. In addition, it is possible to derive the aberration coefficients C_s and $C_c \approx V/F$ in terms of the initial energy and electric field strength at the sample F (V/cm) [7]. These aberrations are derived from the parabolic trajectories in the accelerating field portion of the immersion lens, and are the lowest aberrations possible. Chmelik et al. [11] have shown that for a well designed objective, the actual aberration coefficients approach these values. Given a very narrow energy filter, one can choose $\Delta V_{\min}$ to be low enough to approach the spherical aberration limit. We shall assume that spherical and optimized chromatic aberration terms contribute equally, and choose the analyzer $\Delta V_{\min}$ accordingly. With these modifications to eq. (9), the high-resolution conditions *for imaging* are:

$$\begin{aligned} \alpha_{\mathrm{opt}}^2 &= 0.6K_\lambda F/V^{1/2}\,\Delta V_{\min}, \\ \delta_{\min}^2 &= 2.4K_\lambda\,\Delta V_{\min}/V^{1/2}F, \\ \Omega\,\Delta V &= \pi\alpha_{\mathrm{opt}}^2\,\Delta V_{\min} = 1.88K_\lambda F/V^{1/2}. \end{aligned} \tag{10}$$

In these equations, one should note that overfiltering the image to improve resolution allows larger aperture angles, and does not degrade the collection factor. The very high resolution of cathode lens arises from the high field strength and correspondingly low aberration. For a 100 eV line with a field strength of 10 kV/mm, $C_s \approx C_c \approx 10\ \mu$m, compared to a few centimeters for a good SAM objective. The diffraction limit can only be overcome by using large angles and low aberrations. This emphasizes the importance of high field strengths in the LEEM objective. Resolutions of 3 nm seem possible with suitable samples.

5.4. Optimizing for best collection efficiency

In the somewhat lower resolution range where spectroscopic LEEM is possible, diffraction becomes negligible and spherical and chromatic aberration terms dominate eq. (4). With the substitution $\alpha^2\,\Delta V = y$, the expression for resolution becomes:

$$\begin{aligned} \delta^2 &\approx C_s^2\alpha^6 + C_c^2\alpha^2\,\Delta V^2/V^2 \\ &= C_s^2y^3/\Delta V^3 + C_c^2y\,\Delta V/V^2. \end{aligned} \tag{11}$$

We want to maximize the collection factor y by proper choice of both α and ΔV, while insuring resolution δ is obtained. Considering δ to be a constant, variable $y(\alpha, \Delta V)$ may be maximized by differentiating the equation with respect to ΔV, and realizing that $\partial y/\partial\,\Delta V = 0$ when y is maximum. This gives ΔV as a function of y, which may be inserted into the original equation to find the dependence of optimum ΔV, α and $\Omega\,\Delta V$ as a function of resolution. Again using the approximations for C_s, $C_c \approx V/F$ for imaging:

$$\begin{aligned} \Delta V_{\mathrm{opt}} &\approx 1.08C_s^{1/3}V\delta^{2/3}/C_c \\ &\approx 1.08F^{2/3}V^{1/3}\delta^{2/3} \le \Delta E, \\ \alpha_{\mathrm{opt}}^2 &\approx 0.62\delta^{2/3}/C_s^{2/3} \approx 0.62F^{2/3}\delta^{2/3}/V^{2/3}, \\ \Omega\,\Delta V &= \pi\alpha^2\,\Delta V \approx 2.13V\delta^{4/3}/C_s^{1/3}C_c \\ &\approx 2.13F^{4/3}\delta^{4/3}/V^{1/3}. \end{aligned} \tag{12}$$

These equations give the resolution dependence of collection factor under optimum conditions. Note that when the optimum energy window exceeds the natural linewidth ΔE, the aperture angle α_{opt} should still be used, but the energy window should not exceed ΔE, because otherwise only background is increased. The collection factor becomes

$\Omega\,\Delta V \approx 1.94F^{2/3}\delta^{2/3}\,\Delta E/V^{2/3}$ when $\Delta V > \Delta E$. At 100 nm resolution, typical collection efficiencies are a few percent compared to about 10% for a CMA.

5.5. Optimizing the detector

Both systems need in-vacuum amplification to detect weak images. SAM systems usually use an

Table 1
Definitions of symbols used in the text (numerical assumptions are those used for the comparison in fig. 4, and are discussed in the text)

Symbol	Definition	Units	Numerical assumptions	
			SAM	LEEM
$(S/N)^2$	Square of signal-to-noise ratio in pixel	$(\%)^2$	(result)	
δ	Pixel size or resolution	cm	(variable)	
n^2	Number of pixels in image	units^2	50^2	
Y_S	Quantum yield in Auger line V, ΔE, V_i	%	0.001%	
Y_b	Quantum yield of background V, ΔE, V_i	%	0.01%	
K	$= Y_S/Y_b$ contrast of Auger line V, ΔE, V_i	%	10%	
V	Energy of Auger emission	eV	100	
V_i	Primary illumination energy	eV	3000	
Y_T	Total scattering yield at V_i	%	–	50%
Ω_S	Emission solid angle of Auger background	sr	π	
ΔE	Natural linewidth of Auger line (V, V_i)	eV	2	
T	Total image integration time	s	100	
B_i	Effective illumination brightness at V_i	A/cm^2·sr	10^7	10^5
e	Electronic charge	A·s	1.6×10^{-19}	
C_{si}	Obj. lens spherical aberration at V_i	cm	2	0.5
C_{ci}	Obj. lens chromatic aberration at V_i	cm	1	–
K_1	$= h/\sqrt{2me}$ diffraction constant	cm eV$^{1/2}$	12×10^{-8}	
ΔV_i	Energy spread of gun	eV	1	–
k	Beam interactions factor for optics	cm/A	8.3	
D_{max}	Maximum dose for specimen damage	A·s/cm^2	100	
δ_{min}	Optics-limited ultimate resolution	cm	(result)	
Q	Detection quantum efficiency	%	1.0	
Ω_A	Detection solid angle of SAM analyser	sr	0.314	–
Ω	Acceptance solid angle of cathode lens	sr	(result)	
ΔV	Energy window of LEEM analyser $< \Delta E$	eV	(result)	
F	Field strength at sample of cathode lens	V/cm	–	10^5
ΔV_{min}	Minimum energy window of LEEM analyser	eV	–	0.25
α	Acceptance angle of objective lens	sr	(variable)	

electron multiplier or scintillator/PMT combination. It is fairly easy to approach DQE = $Q = 1$ with these detectors. A SPEC LEEM could use a CCD camera or a microchannel plate intensifier. To cover the sensitivity range requirements of both conventional LEEM/LEED and Auger imaging, a channel plate is favored [6]. However, if these channel plates are placed directly in the 20 keV imaging beam, the low secondary electron yield of the input face of the intensifier can lead to a low DQE.

The most favorable DQE is obtained when the *cumulative* gain following each successive stage of multiplication is substantially larger than one. High gain in the first stage is most important. This assures that each primary gives a narrow pulse height distribution at the output. To fully exploit the SPEC LEEM, the intensifier must meet this criterion. Instead of placing the MCP directly in the beam, a grainless scintillator that is light-optically coupled to a photo catnode/MCP assembly seems desirable. Estimates suggest that this kind of intensifier can approach $Q = 1$ provided that the channel plate operates at high gain.

The equations for signal-to-noise ratio versus resolution according to the models developed in section 4 are given in eqs. (13) and (14).
The dose factors in brackets are appropriate for gun brightness, beam interactions and dose-limited cases, with the understanding that the smallest of the three possible numbers is the dose-limiting factor. Ultimate resolution limits are given separately. For convenience, the definitions of all parameters are given in table 1. To the right are listed numerical assumptions to be used in the next section. These numbers are *not* appropriate for *all* systems, but need to be known to use the model.

6. Performance comparison

This section offers a numerical comparison of SAM versus SPEC LEEM based on the model above. Table 1 gives the numerical assumptions for each parameter. The numbers do not represent a specific specimen or existing systems, and each number is subject to questions not addressed. The

Scanning SAM

$$\left[\frac{S}{N}\right]^2 \le \left[\frac{KY_S}{4\Omega_S\,\Delta E}\right]\left\{\begin{array}{c}\dfrac{1.55B_iT\delta^{8/3}}{eC_{si}^{2/3}n^2}\\[2ex]\dfrac{1.00T\delta}{ekn^2}\\[2ex]\dfrac{D_{max}\delta^2}{e}\end{array}\right\}[Q\Omega_\lambda\,\Delta E], \tag{13}$$

when $\delta^2 > \delta_{min}^2 \approx 1.2K_\lambda C_{ci}\,\Delta V_{ii}/V_i^{3/2}$.

Imaging SPEC LEEM

$$\left[\frac{S}{N}\right]^2 \le \left[\frac{KY_S}{4\Omega_S\,\Delta E}\right]\left\{\begin{array}{c}\dfrac{2.48B_iTn^{2/3}\delta^{8/3}}{eC_{si}^{2/3}}\\[2ex]\dfrac{0.63T\delta}{ekY_Tn^2}\\[2ex]\dfrac{D_{max}\delta^2}{e}\end{array}\right\}\left[\frac{2.13QF^{4/3}\delta^{4/3}}{V^{1/3}}\right], \tag{14}$$

when $\delta^2 > \delta_{min}^2 \approx 2.4K_\lambda\,\Delta V_{min}/V^{1/2}F$,
and $(\Omega\,\Delta V)_{min} \approx 1.88K_\lambda F/V^{1/2}$,
and $(\Omega\,\Delta V)_{max} < 1.94F^{2/3}\delta^{2/3}/\Delta E\,V^{2/3}$, when $\Delta V_{opt} > \Delta E$.

specimen data is thought to be typical for average materials with a few monolayers coverage [3]. The optical data for both systems are the author's best estimate of aggressive but realistic design goals. The goal of this numerical comparison is to illustrate the approximate relationship between the two systems subject to various limitations, giving some indication of future possibilities. Using parameters from specific specimen and systems, one can also use the model to make real comparisons, in which case these results serve as a datum.

Specimen data is gathered from ref. [3], which gives Auger yields and contrasts for bulk surfaces at $V_i = 3$ keV. They vary from 0.01%–1%, implying cross sections of 10^{-21}–10^{-19} cm^2. A yield of 0.001% seems appropriate for a monolayer of a typical material. A contrast of 10% is possible, but is perhaps optimistic for some combinations of materials. The pixel count of 50×50 is chosen so that the comparison between instruments is not too extreme. Beam interaction limitations in the imaging system also favor a lower pixel count than would normally be used for non-spectroscopic SEM or LEEM micrographs.

Optical aberrations and detector DQE values are intentionally optimistic, in order to establish future goals. However, the resolution and collection efficiency of LEEM objective agree reasona-

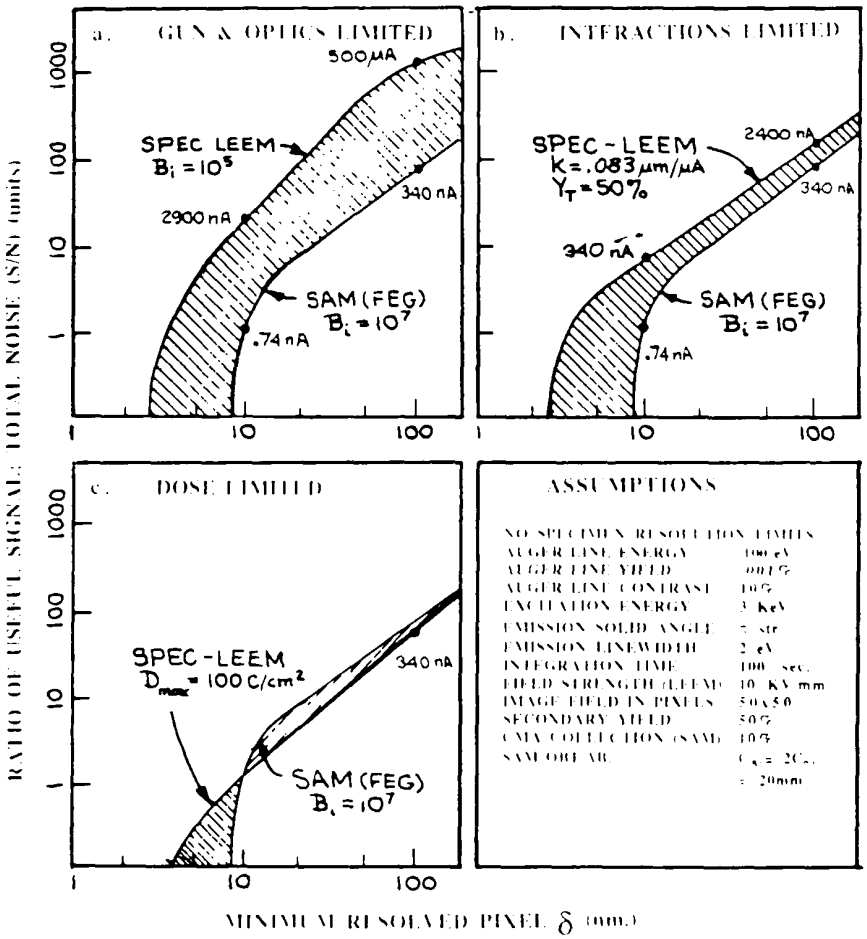

Fig. 4. Comparison of SAM and SPEC LEEM signal-to-noise ratio (S/N) versus resolution calculated from the model and numerical assumptions given in table 1.

bly with a real lens design [11]. It is unlikely that the aberrations of existing non-immersion SAM objective lenses are within a factor of five of what is assumed here. The ultimate resolutions of today's SAM/LEEM systems are about 15 nm instead of the 9.4 and 2.7 nm predicted here. SAM instruments with LaB_6 guns may be expected to deliver about 0.1 nA at 50 nm instead of the 50 nA assumed here. It will also be difficult to design precise setup criteria to insure that optimum conditions are all met simultaneously. This is largely a matter of knowing the exact behavior of the optics from computation. The gun technology required for high-dose factors is much simpler in the imaging instrument.

Figs. 4a–4c show the model results for SAM and LEEM systems with the numbers given in table 1. In fig. 4a, only the gun brightness limits the dose factor. The ultimate resolution of the LEEM is predicted to be 3.5 × better than the SAM because an accelerating immersion lens may be used. In the 10–100 nm resolution range of practical interest, the signal-to-noise ratio is 10–50 × higher for LEEM, which would imply 100–2500 × faster image gathering at fixed resolution, or 3–5 × better resolution at fixed integration time.

Fig. 4b imposes a beam interaction limitation upon both systems. The factor $k = 0.083\ \mu m/\mu A$ is derived from refs. [9,10] for similar beam paths. Nevertheless, the uncertainty in the interactions factor k should be emphasized; but assuming it is correct, the performance of the LEEM is significantly degraded. Subject to the same factor k, the SAM results predict better performance than if it were brightness limited, so the brightness-limited curve from fig. 4a is used for comparison. The SPEC LEEM shows approximately 2 × better resolution and S/N over the range of interest. A factor of 4 faster imaging would be possible. Theoretical ultimate resolution is not limited by beam interactions because the current may be lowered accordingly.

Fig 4c imposes a dose limit of 100 C/cm^2 due to specimen damage. This is the dose delivered by a 1 μA beam of 1 μm diameter for ~ 1 s, which is a fairly typical set of conditions for obtaining full field spectra or very-low-resolution line scans in a SAM. With this severe dose limitation, the relative performance of the two instruments depends entirely upon collection efficiency. However, under the conditions assumed here, the SAM system still remains brightness limited. It is somewhat superior at low resolution because of its higher collection efficiency, but would take much longer to gather the image. In the LEEM, one could decrease the exposure time to match the dose limit, but would have to be satisfied with slightly poorer image statistics. At very high resolution the LEEM retains its advantage.

In general, it is remarkable that the models predict very favorable performance for both instruments. In today's SAM instruments, line scans are usually favored over two-dimensional mapping, because pixel counts are lower and shorter integration times may be used. Nevertheless, line scans or maps with better than 50–100 nm resolution are uncommon, and integration times for maps are usually much longer than 100 s. The high performance of the SAM modeled here is probably due to the combined contributions of many favorable assumptions rather than to one specific factor. In the LEEM, each of the instrumental assumptions seems to be realistic, but the combined conditions will also be difficult to achieve. In an optimized situation, relatively small fractional deviations all contribute negatively to the end result. When many factors are involved, these small deviations multiply to strongly influence the end result.

In fig. 4, the curves scale with the square roots of yield, contrast, linewidth, brightness, solid angles, DQE, and integration time. On the logarithmic scale used, it is relatively easy to shift the curves to match different assumptions. When the curves for a given specimen and instrument configuration are known, they may be used to great advantage in choosing an optimum setup. This procedure works backward from known specimen properties and maximum tolerable integration time. One decides upon a tolerable S/N threshold for distinguishing between two pixels with *different* materials with sufficient statistical confidence. From the curves, one can then decide upon a reasonable resolution goal. From the optimization conditions and the dose-limiting equations, one

may choose the optimum energy window, apertures, magnifications, illuminated area, pixel count, etc., so that the resolution goal is actually met, and so that the collection and illumination are both optimum. The procedure is systematic, although it will undoubtedly be iterative.

In both instruments, the secondary electron image may be used to advantage for specimen survey and optical setup. This image has high yield and contrast for topographic features. The elastic backscatter LEEM and LEED modes also offer complementary data. Given energy filtering, the LEEM as well as SAM can both offer high resolution. In the LEEM, UV-excited PEEM imaging may also be used, giving some degree of chemical sensitivity from work function variations [3]. Since focus, stigmation, alignment and aperture centering will be difficult at integration times necessary for Auger mapping, these complementary, high-bandwidth imaging modes gain practical significance. The product KY_sT in the model is a constant for a given S/N threshold, so that a yield of 10% instead of 0.001% would reduce integration times by a factor of 10^4. In a LEEM or a field emission SAM, secondary images may be obtained at TV rates, allowing real-time adjustments. This has proven to be an enormous practical advantage in mapping work [4].

7. Additional factors influencing visibility

Predictions for resolution and visibility are dangerous because it is certain that they will not be fully realized. In some cases, the specimen may be blamed. For example, significantly better SAM performance has been demonstrated from very thin transmission samples, where background and lateral scattering are suppressed. In a scanning instrument, the instrumental resolution function is convolved with scattering distributions that depend upon both the Auger escape depth and the penetration depth of the primary illumination. The latter dependence arises because Augers are excited not only by incident electrons, but also by backscattered electrons from below, which are generated as the beam is absorbed deeper within the substrate. Additionally, there are difficulties separating topographic from chemical contrast, particularly when the background near a peak is non-uniform, or when underlying chemical and topographic boundaries are not correlated. These "proximity effects" occur because the surface Auger yield can come from areas not directly illuminated by the beam.

From this viewpoint, direct imaging may be advantageous in some cases. Fig. 5 shows the imaging behavior of a thin island of foreign material on a uniform substrate when illuminated by a scanned versus uniform beam. For scanning, the specimen contribution to the resolution function is approximately a double Gaussian distribution, with the narrower peak coming from Augers directly excited by the primary beam, and the wider peak coming from backscatters re-emerging through the surface. The widths of these two Gaussians depends on the Auger escape depth and incident penetration depth, respectively. They can be of similar amplitudes. When scanned across the island of material, an image profile with sharper edges and diffuse tails results. The net effect is to reduce the contrast of closely spaced material boundaries. The effect is similar to the proximity effect encountered in high resolution E-beam lithography.

In the direct imaging case, the illumination from above is uniform, and if the chemical features are thin layers on a uniform substrate, the

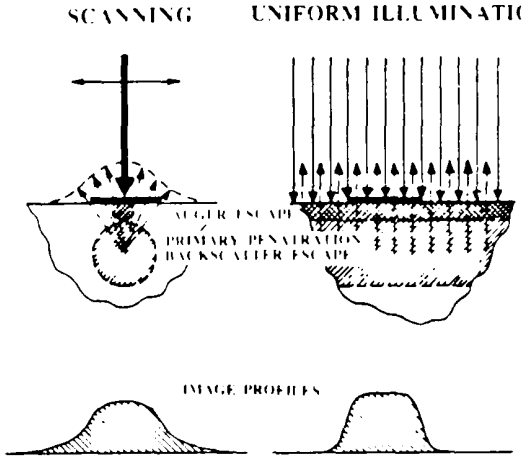

Fig. 5. Proximity effects using scanning versus direct imaging to map an island of thin material on a thick substrate.

backscatter illumination from below is also uniform. The two components of illumination are identical as seen from the surface, and the wider backscatter Gaussian is missing from the resolution function. The image reflects only the effects of the Auger escape depth. This difference could be important when observing epitaxial growth or surface diffusion processes in the two instruments.

As a final consideration, the possibilities for direct imaging of X-ray emissions should be mentioned. In a SPEC LEEM with an immersion cathode lens, the collection factor is favorable for direct imaging ESCA or XPEEM observation [3]. To date, the problem seems to lie in obtaining adequate flux density at the sample. If a focused flux density L (photons/cm^2 · sec) at the sample is available, then the dose factor $LT\delta^2$ may be used in the model to predict XPEEM performance. XPEEM is discussed in more detail by Bauer in ref. [12], along with the application aspects of the spectroscopic LEEM.

8. Summary

A system model for scanning Auger microprobes and spectroscopic direct surface imaging microscopes has been developed and used to compare image statistics versus resolution for chemical mapping. Limitations posed by electron gun brightness, stochastic beam interactions, and specimen damage are considered. Optimum electron optical conditions are derived, allowing setups to be directed towards realistic resolution goals that can be estimated beforehand. In the SPEC LEEM instrument, parallel illumination of many pixels allows very high illumination flux. Net collection efficiency is lower than a SAM, but can be remarkably favorable if an immersion lens with high field strength is used. At high resolution, the imaging energy filter in a SPEC LEEM may be used to optimize collection efficiency while enhancing resolution. Surprisingly, overfiltering leads to better performance, and in general the optimization of both energy window and aperture and field strength are shown to be vital. Ultimate instrumental resolution and contrast of the SPEC LEEM seems to be superior, but predictions are subject to sample limitations. In general, the model predicts higher resolution and shorter integration times than SAM presently achieves. This is attributed to a favorable combination of assumptions that may be realistic, but are not met in either instrument. Due to parallel illumination and imaging, the LEEM promises to be faster, but is subject to stochastic Coulomb interactions that cannot yet be accurately predicted. As is usually the case, these theoretical results will have to await experimental confirmation under tightly controlled conditions. The model serves to guide design decisions and to assist in achieving favorable setups. If instruments confirming these predictions are built, then higher-bandwidth chemical observation of surfaces will become possible.

Acknowledgement

The author thanks E. Bauer for his critique and support.

References

[1] W. Telieps and E. Bauer, Ultramicroscopy 17 (1985) 57.
[2] E. Bauer, M. Mundschau, W. Swiech and W. Telieps, Ultramicroscopy 31 (1989) 49.
[3] E. Bauer and W. Telieps, in: Surface and Interface Characterization by Electron-Optical Methods, Eds. A. Howie and U. Valdre (Plenum Press, 1988) pp. 195–223.
[4] G. Todd, H. Poppa and L. Veneklasen, Thin Solid Films 57 (1979) 213.
[5] L. Veneklasen, G. Todd and H. Poppa, in: Proc. 9th Int. Congr. on Electron Microscopy, Toronto, 1978.
[6] L. Veneklasen, 36 (1991) 76.
[7] E. Bauer, Ultramicroscopy 17 (1985) 51.
[8] T. Mulvey, Electron microprobes, in: Focussing of Charged Particles, Ed. A. Septier (Academic Press, New York, 1967).
[9] L. Veneklasen, N. Yew and J.C. Wiesner, in: Proc. 15th Symp. on Electron, Ion and Photon Beam Technology, Seattle, 1978.
[10] L. Veneklasen, J. Vac. Sci. Technol. B 3 (1985) 185.
[11] J. Chmelik, L. Veneklasen and G. Marx, Optik 83 (1985) 155.
[12] E. Bauer, Ultramicroscopy 36 (1991) 52.